Dalton Transactions

ROYAL SOCIETY OF CHEMISTRY

PAPER

View Article Online
View Journal | View Issue

Cite this: *Dalton Trans.*, 2025, **54**, 11895

Water-mediated isotropic exchange in an extended Cu(II) crystal lattice: a structural, magnetic and EPR study†

Ana L. Pérez, [a] Axel Kemmerer, [a] María de los Milagros Citta,[a] Sebastián Suarez, [b] Ricardo Baggio,[c] Ayelén F. Crespi, [d,e] Juan M. Lázaro-Martínez, [d,e] Carlos A. Ramos,[f] Marcelo Vasquez Mansilla[g] and Carlos D. Brondino *[a]

We report a study to evaluate the relevance of oriented water molecules in the transmission of through-bond isotropic exchange between two distant $S = 1/2$ spins. The study is carried out by means of a structural, magnetic and EPR characterization of the copper compound (pyridine-2,6-dicarboxylato)-(pyridine-2,6-dicarboxylic acid)-copper(II) monohydrate (CuDPA). The structure of this compound consists of an extended lattice of Cu(II) ions ($S = 1/2$, $I = 3/2$) coordinated to two DPA ligands in a tridentate manner, linked by long pathways in which a oriented water molecule connects two covalent moieties. FTIR experiments complemented by DFT calculations confirmed the importance of this water molecule in stabilizing the crystal structure of CuDPA. X- and Q-band CW-EPR experiments on powder and single crystal samples of CuDPA indicated the presence of isotropic exchange interactions strong enough to collapse both the hyperfine structure due to the Cu(II) nuclei and the resonances of magnetically inequivalent Cu(II) ions. Magnetic susceptibility measurements indicated Curie–Weiss behavior in the 1.8–250 K range with antiferromagnetically coupled Cu(II) spins. The crystal EPR data were rationalized using the theory of Kubo and Tomita, considering that the position of the observed Lorentzian exchange-collapsed resonances is determined by the Zeeman Hamiltonian and that their widths arise from perturbations such as dipolar, anisotropic and antisymmetric exchange, hyperfine coupling and **g** anisotropy, all modulated by isotropic exchange. Although information about the molecular $\mathbf{g}_i$ matrices is lost due to exchange averaging, their eigenvalues and eigenvectors could be reconstructed taking into account the symmetry operations in the crystal lattice of CuDPA. The exchange interaction between magnetically inequivalent copper ions was evaluated from the microwave dependent contribution due to the **g** anisotropy contribution to the linewidth. Our analysis revealed that, despite the strong distortion of the Cu(II) site, the magnetic ground state of the Cu(II) ion is primarily of the $d_{x^2-y^2}$ type. We found that water mediates superexchange through a pathway with a through-bond length of ~10 Å with $|J| = 0.0177(7)$ cm^{-1}. The latter demonstrates the importance of structural water molecules in mediating exchange interactions over long distances that are strong enough to determine the spin state of the system.

Received 11th June 2025,
Accepted 14th July 2025

DOI: 10.1039/d5dt01377a

rsc.li/dalton

[a]*Departamento de Física, Facultad de Bioquímica y Ciencias Biológicas, Universidad Nacional del Litoral - CONICET, Ciudad Universitaria, S3000ZAA Santa Fe, Argentina. E-mail: brondino@fbcb.unl.edu.ar*
[b]*Department of Plant Ecophysiology, Faculty of Biology, Adam Mickiewicz University, Uniwersytetu Poznańskiego 6, 61-614 Poznań, Poland*
[c]*Gerencia de Investigación y Aplicaciones, Centro Atómico Constituyentes, Comisión Nacional de Energía Atómica, Buenos Aires, Argentina*
[d]*Universidad de Buenos Aires, Facultad de Farmacia y Bioquímica, Departamento de Ciencias Químicas, 1113 Buenos Aires, Argentina*
[e]*CONICET – Universidad de Buenos Aires, Instituto de Química y Metabolismo del Fármaco (IQUIMEFA-UBA-CONICET), 1113 Buenos Aires, Argentina*
[f]*Centro Atómico Bariloche, Comisión Nacional de Energía Atómica, 8400, S. C. de Bariloche, Río Negro, Argentina*
[g]*Instituto de Nanociencia y Nanotecnología (CNEA-CONICET), Nodo Bariloche, R8402AGP, S. C. de Bariloche, Río Negro, Argentina*

† Electronic supplementary information (ESI) available. See DOI: https://doi.org/10.1039/d5dt01377a

Introduction

The study of exchange-coupled solid-state complexes containing paramagnetic transition metal ions linked by long superexchange pathways is useful for understanding the role that these pathways play in the magnetic properties of these compounds.[1–12] In addition to their essential role in stabilizing the crystal lattice of the compounds, these pathways can also transmit very weak exchange interactions strong enough to change both the spin state and the magnetic dimensionality of the system.[13–17] Transition metal ion centers linked by long superexchange pathways are also essential in proteins involved in bioenergetic cell and enzyme kinetics.[18,19] While the metal centers perform essential functions either as electron transfer centers or as the active site of enzymes, the long chemical link between the centers may act as an electron transfer conduit in addition to its function as a superexchange pathway.[20,21] Thus, the characterization of weakly exchange-coupled systems contributes to our fundamental understanding of magnetic interactions in materials,[4,22] and has potential implications in diverse fields such as the design of organocatalysts,[23–25] the enhancement of electrochemical catalytic reactions at electrode level,[26–29] and particularly in the characterization of long distance electron transfer reactions in biological systems.[21]

Of particular interest in this area is the role of water molecules and hydroxyl ions in transmitting exchange between two metal centers. The characterization of two dinuclear Cu complexes with Cu–OH···O–Cu topologies and Mn(III)/Fe(III) salen-type supramolecular dimers showed the ability of hydrogen bonds to transmit exchange, which was also rationalized by theoretical calculations.[30–36] Interesting examples of water-mediated exchange-coupled systems are the Cu metal sites of the enzymes multi-copper oxidase and peptidylglycine a-hydroxylating monooxygenase, where theoretical calculations showed that water transmits relatively strong ferromagnetic exchange interactions.[37] The role of water has also been investigated in several experiments that suggest that ordered water can mediate electron transfer reactions in redox proteins, providing an indirect evidence that water could act as an efficient superexchange pathway.[25,38–48] However, the role of water as part of long superexchange pathways has received less attention, and to the best of our knowledge, neither experimental nor theoretical work has evaluated the situation. The objective of this work is to evaluate the transmission of exchange mediated by an oriented water molecule bridging two covalent moieties through hydrogen bonds.

Pyridine-2,6-dicarboxylic acid, also known as dipicolinic acid or DPA, is a biologically relevant versatile metal ligand that gives rise to metal compounds with different structural phases.[49–54] Its rigid planar structure with a central pyridine ring flanked by two carboxylate groups promotes specific metal–ligand geometries while facilitating the formation of extended networks through secondary interactions. When coordinated to Cu(II) ions, this ligand binds in a tridentate fashion, but can form complexes with either one or two dipicolinate molecules per Cu(II) center, leading to different crystalline phases with distinct magnetic behaviors and providing an excellent platform for the study of structure–property relationships in weakly exchange-coupled systems.[55–59] In particular, the compound (pyridine-2,6-dicarboxylato)-(pyridine-2,6-dicarboxylic acid)-copper(II) monohydrate consists of an extended lattice of mononuclear Cu(II) ion complexes in which two DPA ligands coordinate tridentate to each Cu(II) center. The crystal lattice of these compounds is stabilized by a single water molecule linking two covalent moieties between pairs of copper centers, making a suitable model system for evaluating exchange interactions mediated by ordered water molecules through long distances.

We report here structural, magnetic and EPR studies of (pyridine-2,6-dicarboxylato)-(pyridine-2,6-dicarboxylic acid)-copper(II) monohydrate, hereafter CuDPA. Magnetic susceptibility measurements are used to reveal the sign of J. Powder and single crystal X- and Q-band CW-EPR are used to evaluate the electronic properties of individual Cu(II) ions and the exchange parameters associated with the superexchange pathways, using a model based on the theory of Kubo and Tomita.[60] All this information, complemented by a detailed study of the crystal structure of CuDPA, allowed us to determine the importance of an oriented water molecule bridging two covalent moieties for the transmission of long-range exchange interactions.

Results and discussion

Crystal and molecular structure of CuDPA

Both powder diffractogram and single crystal X-ray analysis confirmed that the structure of the synthesized compound corresponds to that reported by Sileo *et al.*[50] (Fig. S1†). The same structure has also been described in X-ray studies of varying quality[53,61–63] in CSD.[64] CuDPA crystallizes in the orthorhombic system, space group *Pnna*, $Z = 4$. The complex features a central Cu(II) ion lying on a twofold axis coordinated to two dipicolinic acid molecules, one fully deprotonated and the other fully protonated (Fig. 1). The Cu(II) ions are in a distorted octahedral environment coordinated to four carboxylic oxygen atoms (O1, O1A, O3 and O3A) and to two pyridine nitrogen atoms (N1 and N2, also lying on the twofold axis). The equatorial ligand positions are occupied by atoms N1, O1, and O1A from one dipicolinate molecule and N2 from an adjacent dipicolinic acid molecule.

All equatorial atoms, including Cu, are coplanar with bond distances of Cu1–O1 = Cu1–O1A = 2.008(13) Å, Cu1–N1 = 1.911 (14) Å, and Cu1–N2 = 2.011(14) Å. The direction N1–Cu–N2 forms a C_2 axis of symmetry lying along the *c*-crystal axis. As predicted by the Jahn–Teller effect, oxygen atoms from the protonated dipicolinic acid molecule occupy the apical positions of the octahedron because oxygen atoms from carboxylic acids are weaker donors than oxygen atoms from carboxylates (Cu1–O3 and Cu1–O3A distances are 2.425(13) Å).

Since the space group *Pnna* is centrosymmetric, the four Cu(II) complexes in the unit cell, hereafter referred to Cu1 (x, y,

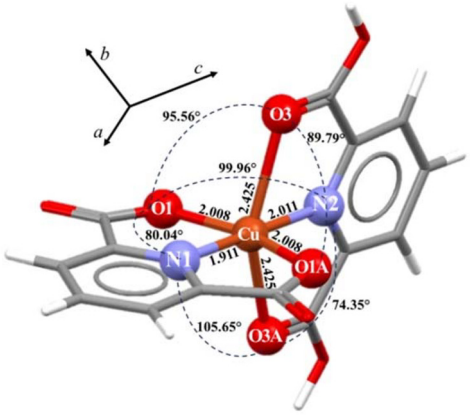

Fig. 1 Coordination around the Cu(II) ion of CuDPA with the Cu–ligand distances in Å and bond angles.

z), Cu2 ($\frac{1}{2}+x, y, -z$), Cu3 ($x, \frac{1}{2}-y, \frac{1}{2}-z$), and Cu4 ($\frac{1}{2}+x, \frac{1}{2}-y, \frac{1}{2}+z$) (Fig. 2), are related in pairs by crystallographic inversion centers, at (1/2, 0, 0) and (1/2, 1/2, 1/2), respectively (Cu1 with Cu2, and Cu3 with Cu4), see Table S1.† This indicates that the putative four magnetically inequivalent Cu centers present in the unit cell of CuDPA can be analyzed from a magnetic point of view as two magnetically inequivalent centers (Fig. S2†).

The Cu(II) centers of CuDPA are connected by a complex network of pathways that give rise to the 3D structure of the crystal lattice (Fig. 2 and Table 1). Cu1 and Cu3, as well as Cu2 and Cu4, (d_{Cu-Cu} = 5.968, 7.890 and 9.893 Å) interact through composite pathways that form corrugated layers perpendicular to the c-crystal axis. Remarkably, a single structural water molecule is involved in the hydrogen bond mediated pathways connecting the Cu(II) ions situated in each layer (Fig. 2, panels A and B). The potential superexchange pathways mediated by this water molecule are labeled $J_{1,3-5}$ in Fig. 2 and Table 1.

Magnetically equivalent sites belonging to different layers (Cu1–Cu2, and Cu3–Cu4, d_{Cu-Cu} of 7.385 Å), are connected by hydrophobic interactions mediated by the aromatic ring of unprotonated DPA molecules (ring–ring distances of 3.417 Å). This interaction forms zigzag chains along the crystallographic a-axis, in which the putative superexchange pathway is identified as J_6 in Fig. 2 and Table 1.

ATR-FTIR: relevance of the oriented water molecule in the lattice stabilization

To study the contribution of the structural water molecule to the stability of CuDPA, we performed ATR-FTIR measurements on samples of CuDPA (see Experimental section for details) (Fig. 3). CuDPA showed characteristic signals due to the symmetric (ν_{sym} = 1330 and 1340 cm^{-1}) and asymmetric (ν_{as} = 1672 and 1652 cm^{-1}) stretching of the carboxylate groups (RCO_2^-) and of the carbonyl of the carboxylic acids (RCO_2H) at ~1700 cm^{-1}, which coordinate with the Cu(II) ions and are hydrogen-bonded to the structural water molecules. The difference in absorption values for the carboxylate groups ($\Delta\nu_{as-sym}$ = 322 and 342 cm^{-1}) indicates that the coordination

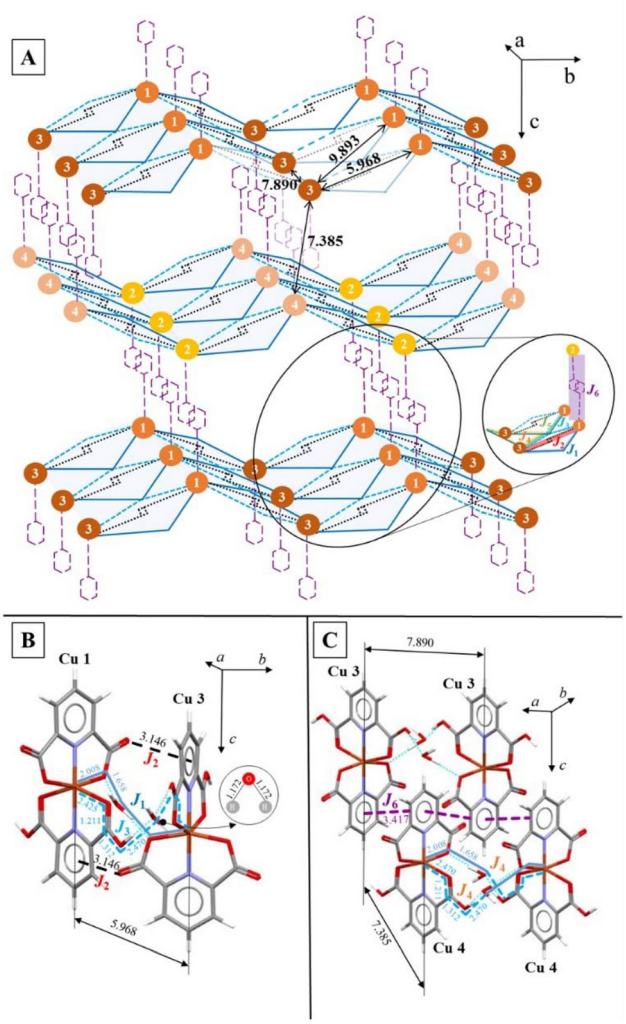

Fig. 2 Panel A shows a schematic view of the 3D structure of CuDPA with all the links between Cu sites. Panel B shows the CO–π (J_2) and hydrogen bond mediated bonds between magnetically inequivalent sites (J_1 and J_3). Panel C shows the links between magnetically equivalent sites. These links involve two types of interactions: π–π stacking (J_6) and hydrogen bonds (J_4).

Table 1 Description of the links between Cu(II) ions in CuDPA indicating the nature, apical or equatorial, of the copper ligands and the type of non-covalent interaction involved

Exchange constant	Non-covalent interaction	Atoms involved	d_{Cu-Cu} (Å)
J_1	Hydrogen bond	Cu_3–$O1_{eq}$···H_w–O_w–H_w···$O1A_{eq}$–Cu_1 (Cu–Cu through bond distance, d = 9.676 Å)	5.968
J_2	CO–π		5.968
J_3	Hydrogen bond	Cu_3–$O3_{ap}$–C8–O4–H5···O_w···H5A–O4A–C8A–O_{ap}–Cu_1 (d = 14.836 Å)	5.968
J_4	Hydrogen bond	Cu_3–$O3_{ap}$–C8–O4–H5···O_w–H_w···$O1_{eq}$–Cu_3 (d = 12.256 Å)	7.890
J_5	Hydrogen bond	Cu_3–$O3_{ap}$–C8–O4–H5···O_w–H_w···$O1A_{eq}$–Cu_1 (d = 12.256 Å)	9.893
J_6	π–π stacking		7.385

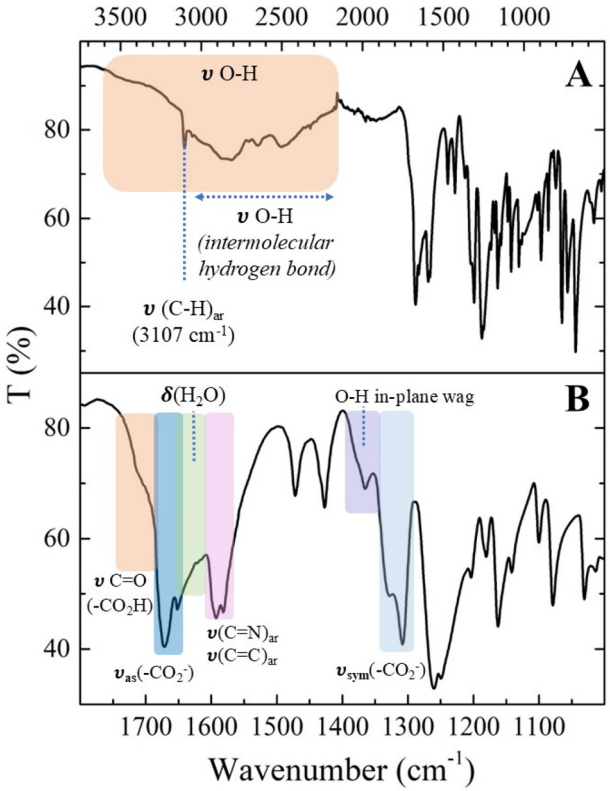

Fig. 3 Total (A) and partial (B) ATR-FTIR spectrum for crystalline samples of CuDPA.

of the Cu(II) metal ion is of the monodentate type, in agreement with the X-ray single crystal structure.[65] The stretching of the aromatic ring ($\nu_{(C=N/C=C)ar}$) is also observed at 1592 and 1582 cm^{-1} and the stretching of the C–H bond of the pyridinic ring is present at 3107 cm^{-1}.[66,67] In addition, the stretching of the OH groups is seen at frequencies between 3500 and 2150 cm^{-1}. This frequency range, which is lower than the usual one above 3000 cm^{-1} for the OH groups, is indicative of a strong intermolecular hydrogen bonding network.

Due to the intensity of the bands associated with the carboxylate groups, it is difficult to distinguish the contribution associated with the bending of the structural water molecules. Therefore, we performed theoretical calculations based on DFT to rationalize the importance of the structural water molecules in stabilizing the crystal lattice. The calculations predicted the experimental FTIR data reasonably well, using as a model the reported X-ray structure of CuDPA (Table S2†). However, the same calculations performed in the absence of water molecules showed drastic changes in the arrangement of the Cu(II) ion complexes and hence in the predicted IR spectrum (Tables S3 and S4†). Taken together, ATR-FTIR and computational calculations indicate the important role of the structural water molecule in stabilizing the crystal structure of CuDPA and thus its relevance as a linker of the Cu(II) ions.

Magnetic susceptibility measurements

Temperature-dependent magnetic susceptibility (χ) measurements of a powder sample of CuDPA are shown in Fig. 4. CuDPA exhibited Curie–Weiss behavior typical of mononuclear Cu(II) ions ($S = 1/2$) weakly coupled by exchange. The Curie–Weiss model can be rationalized with the spin Hamiltonian $H = \mu_B g S_z B - zJ\langle S\rangle_z S_z$. The first term represents the Zeeman interaction assuming Cu(II) centers with isotropic g-value. The second term accounts for intermolecular exchange interactions using the molecular field approximation. In this model, μ_B is the Bohr magneton, B is the external magnetic field, S_z is the spin operator associated with each spin of the crystal lattice, $\langle S_z\rangle$ is the mean value of the z-component of the spin operator, J is the isotropic exchange parameter between nearest-neighbor magnetic species, and z is the number of first neighbors surrounding each Cu(II) center. Analysis of these data with this model yielded $C = 0.4366(1)$ emu K mol^{-1} and $\theta = -0.17(3)$ K, indicating weak antiferromagnetic interactions. An isotropic value of $g = 2.1576(5)$ was obtained from the Curie constant. Taking into account the θ value, we calculated $zJ = -0.46(8)$ cm^{-1} using molecular field theory (note that z includes both magnetically equivalent and nonequivalent Cu(II) ions).

EPR measurements: powder and single crystal EPR spectra

X- and Q-band powder EPR spectra of CuDPA are shown in Fig. 5. Both spectra are typical of an extended lattice of $S = 1/2$ spins coupled by exchange. The Q-band spectrum shows rhombic symmetry with no evidence of hyperfine structure with the Cu(II) nuclei. Single crystal EPR spectra at X- and Q-band and at room temperature showed a single Lorentzian resonance line with no evidence of hyperfine structure for all tested magnetic field directions (Fig. S3† panel A and B). The single crystal EPR experiment, in agreement with the powder EPR spectra, indicates the presence of strong enough exchange interactions to collapse both the hyperfine structure with the

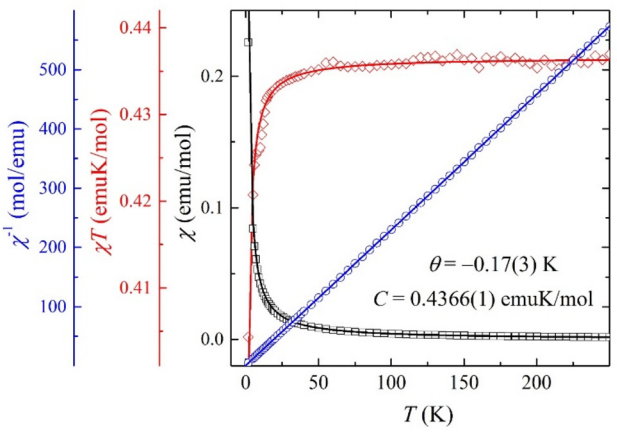

Fig. 4 Plot of the χ, χT and $\chi^{-1}(T)$ *vs.* T for CuDPA. Parameters were obtained by least squares fitting of a Curie–Weiss model to the data. Curie–Weiss analysis was performed in the temperature range of 1.8 to 250 K.

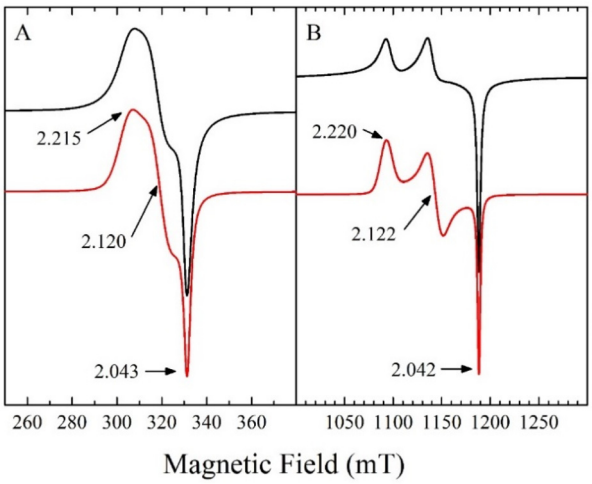

Fig. 5 Powder EPR spectra of CuDPA at room temperature together with simulation (red solid lines). The EPR parameters used in the simulation were $g_{1,2,3}$ = 2.215, 2.120, 2.043 for X-band (panel A) and $g_{1,2,3}$ = 2.220, 2.122, 2.042 for Q-band (panel B).

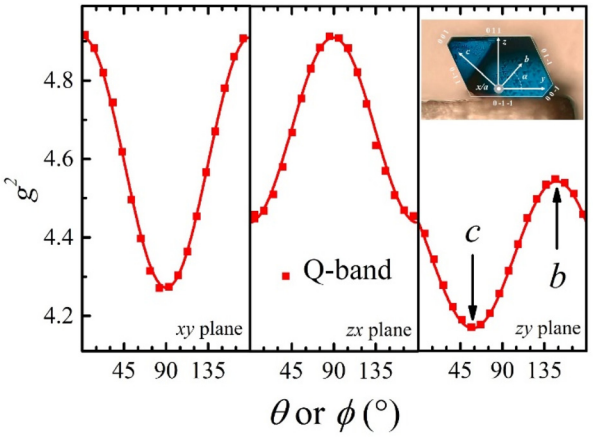

Fig. 6 Q-band angular variations of g^2 values in three crystal planes of CuDPA. The inset on the figure shows the mounting of a single crystal sample and indicates the relative position of the crystal axes with respect to the lab frame. The solid lines are obtained by least squares fitting the function $g^2(\theta,\phi)$ = **h**·**g**·**g**·**h**, where **h** = **B**/|**B**| is the magnetic field direction in the lab frame, to the data. The X-band data along with the fit are shown in Fig. S4.†

Cu(II) nuclei and the resonances of the magnetically inequivalent Cu(II) ions. More specifically, this collapse affects the resonances of Cu1 and Cu3, as well as Cu2 and Cu4 (Fig. 2).

The crystal g matrix. For an extended lattice of four S_i = 1/2 spins per unit cell with resonance lines collapsed by exchange, the position of the resonances is given by the Zeeman spin Hamiltonian

$$H_z = \mu_B \mathbf{S} \cdot \mathbf{g} \cdot \mathbf{B} \quad (1)$$

In eqn (1), **S** is the total spin obtained as $\mathbf{S} = \sum_{p,i=1-4} S_{pi}$, with the sum being over all the unit cells (p) of the crystal, **g** = (**g**$_1$ + **g**$_2$ + **g**$_3$ + **g**$_4$)/4 is the crystal **g** matrix, where **g**$_i$ are the molecular matrices, and **B** is the external magnetic field in the lab frame. Since Cu1 and Cu2, as well as Cu3 and Cu4, are related by an inversion, they are magnetically equivalent for the EPR experiment (**g**$_1$ = **g**$_2$ and **g**$_3$ = **g**$_4$) and hence **g** = (**g**$_1$ + **g**$_3$)/2.

We determined **g**^{2} (**g**^{2} = **g**·**g**) from the position of the single exchange collapsed resonances obtained in three crystal planes of CuDPA (Fig. 6, S3 and S4†).

The **g**^{2} components of CuDPA in the lab frame, together with their eigenvalues and eigenvectors are given in Table 2. As shown in Fig. 6 and S4,† the **g**^{2} angular variation at both X- and Q-band follows the symmetry of the orthorhombic lattice of CuDPA, *i.e.* the C_2 symmetry around the three crystal axes of CuDPA.

In parallel, we simulated the well-resolved powder Q-band EPR spectrum of CuDPA with the Zeeman Hamiltonian of eqn (1) (Fig. 5). The parameters obtained were $g_{1,2,3}$ = 2.220, 2.122, 2.042. These g values were used as starting values to simulate the less resolved X-band spectrum, which yielded $g_{1,2,3}$ = 2.215, 2.120, 2.043. The similarity of the g-values obtained for the powder samples to the eigenvalues of the crystal **g** matrix, as determined by single crystal EPR spectroscopy, confirms that the spectra shown in Fig. 5 reflect the symmetry of the crystal lattice rather than that of the individual Cu(II) ions.

Table 2 Crystal and molecular **g**^{2} matrix components of CuDPA in the lab frame together with eigenvalues and eigenvectors. Molecular eigenvectors correspond to Cu1 of the unit cell

Crystal g^2 matrix	
X-band/Q-band	
g_{xx}^2 = 4.917(2)/4.910(3)	g_{xy}^2 = 0.000(2)/0.002(3)
g_{yy}^2 = 4.312(2)/4.272(2)	g_{zx}^2 = −0.002(2)/0.003(3)
g_{zz}^2 = 4.443(2)/4.439(3)	g_{zy}^2 = −0.171(2)/−0.168(3)
g_1 = 2.0480(7)/2.0416(7)	**a**$_1$ = [0.0012(7), 0.824(2), 0.567(3)]/[−0.005(4), 0.850(3), 0.527(5)]
g_2 = 2.1356(7)/2.1314(7)	**a**$_2$ = [0.006(6), −0.567(3), 0.824(2)]/[−0.006(8), −0.527(5), 0.850(3)]
g_3 = 2.2173(5)/2.2159(7)	**a**$_3$ = [−1.00000(3), −0.002(4), 0.006(6)]/[−1.00000(8), −0.001(5), −0.008(7)]
Molecular g$_i^2$ matrix	
X-band/Q-band	
g_{ixx}^2 = 4.918(4)/4.910(4)	g_{ixy}^2 = −0.268(4)/−0.255(4)
g_{iyy}^2 = 4.312(5)/4.272(5)	g_{izx}^2 = 0.388(4)/0.413(4)
g_{izz}^2 = 4.442(5)/4.438(5)	g_{izy}^2 = −0.171(5)/−0.166(5)
g_{i1} = 2.290(3)/2.290(3)	**a**$_{i1}$ = [0.823(2), −0.568(2), 0.0000(5)]/[0.823(2), −0.568(2), 0.000(2)]
g_{i2} = 2.058(3)/2.051(3)	**a**$_{i2}$ = [−0.3227(9), −0.467(2), 0.823(3)]/[−0.2984(9), −0.433(1), 0.851(2)]
g_{i3} = 2.048(3)/2.042(3)	**a**$_{i3}$ = [0.468(1), 0.677(2), 0.568(2)]/[0.483(1), 0.700(2), 0.526(2)]

The molecular g$_i$ matrix. The fact that the crystal **g** matrix is given by **g** = (**g**$_1$ + **g**$_3$)/2 means that some of the information about the molecular **g**$_i$ matrices is lost by averaging. However, since the N1–Cu–N2 direction of the four Cu(II) sites of the unit cell lies on a C_2 symmetry axis coinciding with the c-crystal axis, the crystal g_c value (g_c = g_1 = 2.0480 at X-band,

see Table 2) must correspond to one of the molecular eigenvalues with the corresponding eigenvector lying on the N1–Cu–N2 direction. Given the above, we first calculated the molecular $\mathbf{g}_i^2$ matrices from the crystal $\mathbf{g}^2$ matrix assuming a Cu(II) site with axial symmetry with $g_\perp = g_{i1}$.

The molecular $g_\parallel$ value was obtained from the invariance of the trace of a symmetric matrix upon rotation, *i.e.* Tr $\mathbf{g}^2$ = Tr$\mathbf{g}_i^2$ = ${g_\parallel}^2 + 2\,{g_\perp}^2$ ($g_\parallel$ = 2.299/2.298 at X/Q band with the $g_\parallel$ eigenvector lying along the normal to the Cu(II) site). To verify the validity of the axial symmetry assumption, the diagonal molecular $\mathbf{g}_i^2$ matrices obtained for the two inequivalent Cu(II) ions in the molecular frame were then calculated in the lab frame and the predicted $g_i^2(\theta,\phi)$ values were plotted together with those of the crystal $\mathbf{g}^2$ matrix (Fig. S5†). As shown in this figure, there is a good agreement between calculation and experiment but with some small discrepancies, indicating that the axial model needed some corrections. The latter was considered upon small break of the axial symmetry, searching for the ${g_{i2}}^2$ and ${g_{i3}}^2$ eigenvalues and eigenvectors that gave the best agreement with the experimental data (Fig. 7 and Table 2). This procedure allowed us to conclude that the magnetic ground state of the Cu(II) ion is mainly of the $d_{x^2-y^2}$ type, despite the strong distortion of the Cu(II) site. This was confirmed by DFT calculations that yielded a SOMO orbital predominantly of the $d_{x^2-y^2}$ type (Fig. S6†).

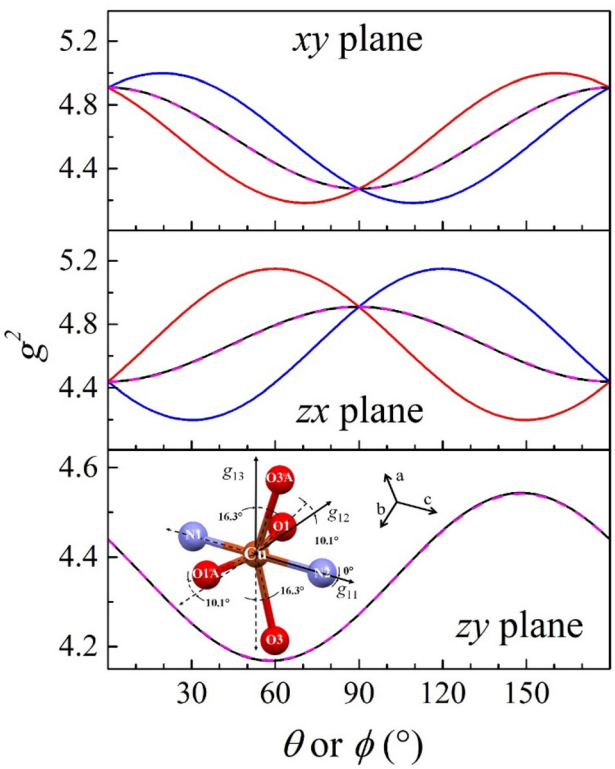

Fig. 7 Theoretical angular variation in the lab frame of the molecular g_i^2 values predicted with the parameters listed in Table 2 (Cu1=Cu2 in red, Cu3=Cu4 in blue). X-band results are shown as ESI (Fig. S7†). The averages of the molecular g_i^2 values of the magnetically inequivalent Cu (II) sites are plotted in magenta (dashed line) together with the crystal g^2 values in black. The four Cu(II) sites are magnetically equivalent in the *zy* plane (magenta) (Fig. S2†).

Linewidth analysis and exchange interaction between magnetically inequivalent Cu(II) ions. The spin Hamiltonian governing the EPR absorption spectrum of an extended lattice with a single exchange-collapsed absorption can be written as

$$H = H_z + H_{ex} + H' \qquad (2)$$

where H_z was defined in eqn (1), H_{ex}, $H_{ex} = -\sum_{i<j} J_{ij} S_i \cdot S_j$, is the HDVV Hamiltonian between the spins localized at the Cu(II) sites i and j of the lattice, and H' is a perturbation. H' includes interactions such as dipolar, anisotropic and antisymmetric exchange, hyperfine coupling, and **g** anisotropy.[68]

The contributions to the EPR linewidth of the different interactions in extended lattices can be rationalized on the basis of Kubo and Tomita and Anderson theories, in which the H' terms are taken as perturbations to H_z + H_{ex} (eqn (2)).[60,69] For 3D extended lattices with a single absorption line narrowed by exchange, the theory predicts inhomogeneously broadened Lorentzian resonances with positions given mainly by H_z (eqn (1)) and linewidths proportional to $\sum$ M2/J, where M2 is the second moment of each interaction contributing to H'. While H' terms give broadening, isotropic exchange gives narrowing.

Fig. 8 shows the angular variation in the lab frame of the EPR peak-to-peak linewidth ($\Delta B_{pp}(\theta,\phi)$) of the single exchange collapsed resonance of CuDPA. The angular variation of X-band $\Delta B_{pp}(\theta,\phi)$ (Fig. 8) resembles that of the crystal $g^2(\theta,\phi)$ (Fig. S4,† top panel). This is not the case of $\Delta B_{pp}(\theta,\phi)$ at Q-band (Fig. 8), which shows significant changes in both values and angular variation due to the higher frequency. This frequency dependent contribution to the linewidth (**g** anisotropy contribution) is detected in the *xy* and *zx* planes but not in the *zy* planes, indicating that it is only observed in those planes containing two magnetically inequivalent Cu(II) ions.

The **g** anisotropy contribution to the linewidth for the case of four spins per unit cell in which $\mathbf{S_1} = \mathbf{S_2}$ and $\mathbf{S_3} = \mathbf{S_4}$ is $H' = \mu_B(\mathbf{S_1} - \mathbf{S_3})(\mathbf{g_1} - \mathbf{g_3})\mathbf{B}$ is given by[70,71]

$$\Delta B_{pp}(\theta,\phi) = \frac{\sqrt{\frac{2}{3}}\pi\omega_o{}^2 h}{8\pi g^3 \omega_e \mu_B}[g_1(\theta,\phi) - g_3(\theta,\phi)]^2 \qquad (3)$$

where ω_o is the Larmor frequency ($\omega_o = 2\pi \times 34$ GHz at Q-band), g is the isotropic crystal g value, and ω_e is the exchange frequency, which is related to the exchange parameters coupling the Cu(II) ions. Note that this equation is independent of the convention used for the exchange Hamiltonian ($H = -J\,S_i\,S_j$ or $H = J\,S_i\,S_j$).[70]

A least squares fitting of the function given in the caption to Table 3 to the X-band $\Delta B_{pp}(\theta,\phi)$ data (Fig. 8) yielded the parameters listed in the table. The Q-band data were least squares fitted with this function and Γ_{1-4} X-band parameters plus eqn (3) to account for the **g** anisotropy contribution observed in the *xy* and *zx* planes (Γ_5 parameter in Table 3). Note that the contributions to the linewidth at X-band are not

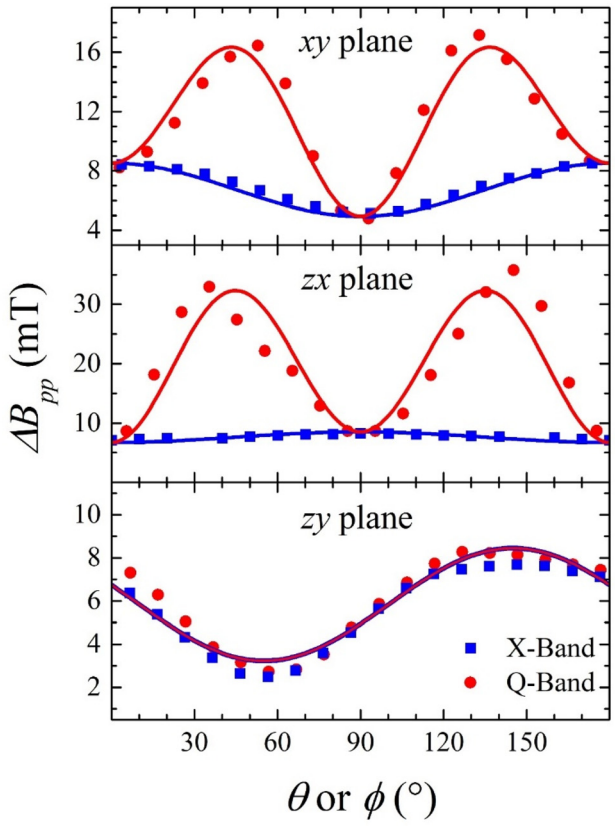

Fig. 8 Angular variation of the linewidth data at X- and Q-band (blue and red) in three crystal planes of CuDPA. The solid lines were obtained with the Γ_i parameters and function given in Table 3.

Table 3 Γ_i parameters obtained by least squares fitting the function $\Delta B_{pp}(\theta,\phi) = \Gamma_1 \sin^2\theta\cos^2\phi + \Gamma_2 \sin^2\theta\sin^2\phi + \Gamma_3\cos^2\theta + \Gamma_4 2\sin\phi\sin\theta\cos\theta + \Gamma_5[g_1(\theta,\phi) - g_3(\theta,\phi)]^2$ to the EPR linewidth data in Fig. 8. The Γ_{1-4} parameters correspond to linewidth contributions due to interactions such as unresolved hyperfine structure and anisotropic and antisymmetric exchange, while Γ_5 weights the **g** anisotropy contribution. The Γ_{1-4} parameters were obtained from a least squares fitting the X-band linewidth data and were used to obtain the **g** anisotropy contribution at Q-band

Γ_i parameters (mT)	
Γ_1	8.5(1)
Γ_2	4.9(1)
Γ_3	6.7(1)
Γ_4	−4.9(2)
Γ_5	n.d. (X-band)/670(30) (Q-band)

significantly changed at Q-band, as shown by the data in the *zy* plane. The value determined for Γ_5 and eqn (3) allowed us to obtain $w_e = 0.025(1)$ cm^{-1}. This w_e value corresponds to the interference of the subpathways J_1, J_2, J_3 and J_5 (see Fig. 2 and Table 1), confirming that the structural water molecule plays an essential role in transmitting exchange. However, the analysis summarized in Table 1 indicates that J_2, J_3 and J_5 can be neglected compared to J_1 because the CO–π interaction (J_2) is a very weak interaction and J_3 and J_5 involve ap–ap and eq–ap ligand–Cu(II) bonds, respectively.

Thus, the fact that only J_1 involves equatorial ligands to Cu(II) indicates that this is the main superexchange pathway between magnetically inequivalent Cu(II) centers, since it is the only subpathway that involves a direct interaction between the $d_{x^2-y^2}$ orbitals of neighboring magnetically inequivalent Cu(II) ions. This interpretation was additionally confirmed by DFT calculations that showed that the unpaired spin density is localized mainly on the equatorial ligand plane of the copper centers (Fig. S6†). Under this assumption, $\omega_e{}^2 = \frac{2J_1{}^2}{\hbar^2}$, then $|J_1| \sim 0.0177(7)$ cm^{-1}.

It is important to note that, while π–π stacking (J_6) couples magnetically equivalent Cu(II) centers and contributes to the Weiss constant ($\theta = zJS(S+1)/3k$)[72,73] (along with all other exchange pathways J_1–J_5), it is not involved in the **g** anisotropy contribution to the EPR linewidth. In other words, the frequency-dependent EPR linewidth can only be attributed to the interaction of **g** anisotropy and the exchange pathways between magnetically inequivalent Cu(II) ions.

Concluding remarks

This paper presents a comprehensive structural, magnetic, and EPR study of an extended lattice of copper complexes in which the metal centers are coupled by water-mediated long-range isotropic exchange interactions.

Although obtaining these results involved the complementary use of magnetic and EPR techniques, the most important of them is single crystal EPR spectroscopy, since it allowed us to evaluate with high precision J constants lower than 1 cm^{-1} at room temperature. It is also important to note that this result could only be obtained by analyzing the data with the exchange narrowing theory of Kubo and Tomita for the case where the exchange collapsed resonance lines undergo broadening due to the inequivalence of the magnetic ions of the lattice.

The main conclusion of the paper is that an oriented water molecule connecting two covalent moieties through hydrogen bonds constitutes an antiferromagnetic superexchange pathway strong enough to collapse both the hyperfine structure and the magnetically inequivalent copper ions into a nearly Lorentzian shape resonance line, thus determining the transition from 0D to 3D magnetic dimensionality of the system.

Remarkably, the superexchange is mediated by a mixed covalent and non-covalent pathway with a through-bond length of ~10 Å and a $|J| \sim 0.0177(7)$ cm^{-1}. This demonstrates the importance of water molecules linked through non-covalent interactions in determining the spin state of the system. Furthermore, this J value predicts maximum electron transfer rates of ~10^{11} s^{-1} between two redox centers, which is much higher than the values typically reported in biological copper systems.[20,74] In conclusion, the ability of water to transmit long-range isotropic exchange interactions confirms its

potential to efficiently mediate electron transfer reactions over long distances.

Experimental section

Materials

All chemicals were of commercially available reagent grade and were used as received. The synthesis of CuDPA was performed as reported elsewhere but with some modifications. $Cu(CH_3COO)\cdot H_2O$ (1 mmol, 0.1996 g, Fluka) and dipicolinic acid (2 mmol, 0.3342 g, Sigma-Aldrich) were dissolved in 100 mL of water. The mixture was stirred at 50 °C until dissolution. The solution was filtered through a 0.22 μm Millipore cellulose nitrate membrane and allowed to evaporate slowly at 40 °C in an oven. After two weeks, blue prismatic single crystals were obtained, which were filtered, washed with a small amount of cold water, and air dried.

Single crystal structure and morphology

Powder X-ray diffraction measurements were performed on a Panalytical Empyrean powder diffractometer using Cu Kα1 radiation (λ = 1.54 Å) and equipped with a PIXcel3D area detector. Data were collected in the range of 5 to 50 degrees (2θ) in an $\theta:2\theta$ configuration, with a step size of 0.026 degrees and a counting time of 200 seconds per step. The sample was placed on a zero background silicon sample holder. The instrument was calibrated against a silicon standard.

Suitable single crystals were mounted and data were collected at room temperature using a Gemini A diffractometer, Oxford Diffraction, Eos CCD detector with graphite-monochromated CuKα (λ = 1.54184 Å) radiation, available at INQUIMAE (FCEN-UBA). CrysAlisPro software, from Oxford Diffraction, was used to collect initial frames for the determination of the unit cell, and subsequently, the program was used to plan data collection.[75] After collection, data reduction was carried out in the CrysAlisPro suite, and multiscan absorption correction was carried out.

ATR-FTIR experimental

ATR-FTIR spectra were recorded on a Nicolet iS50 spectrometer (Thermo Scientific) using a one-reflection diamond crystal with 64 scans at a resolution of 4 cm^{-1}.

Theoretical calculations

DFT calculations were performed with Gaussian 16 using the UB3LYP hybrid functional. The LANL2DZ basis set (ECP for Cu) and 6-31++G(d) (N, O, C, H) were employed.[76] To obtain a precise geometry and electronic structure for the IR calculations, spin density and orbital information, the geometry optimization was performed employing the crystallographic X-ray data and using the unrestricted B3LYP (Becke Three-parameter Lee–Yang–Parr)[77,78] exchange correlation functional with the LANL2DZ basis set for Cu and 6-31++G** for C, H, O and N. This setting led to an optimized complex within a non-computationally demanding scheme that maintained the experimental X-ray structure. The IR spectra were calculated employing the same level of theory for the optimization. In addition, the TZVP and 6-31G bases were evaluated for the optimization of the complex (for light atoms), but the best results were obtained with the base finally used. Moreover, to complement the structural minimization based on X-ray data, the geometry of the same complex was optimized excluding the water molecule that interacts with the carboxylate groups and protonating the deprotonated DPA molecule.

EPR measurements

X- and Q-band CW-EPR spectra were performed on a Bruker EMX-Plus spectrometer equipped either with either nitrogen continuous-flow cryostat (100–340 K) and rectangular cavity and 100 kHz field modulation.

Single crystal of CuDPA was oriented by gluing its (0–1–1) plane to a cleaved KCl cubic holder defining a set of orthogonal *xyz* lab axes. The *x*-axis corresponds to the crystal *a*-axis, while $y = b \times [0, \cos(-57.05°), \sin(-57.05°)]$ and $z = c \times [0, -\sin(-57.05°), \cos(-57.05°)]$. The orientation of the unit cell with respect to the macroscopic single crystal is shown in the inset of Fig. 6. The sample holder was positioned at the center of the microwave cavity as described elsewhere,[79] and rotated with the magnetic field in the *xy*, *zx* and *zy* planes at 10° intervals. The resulting data (Fig. 6 and 8) were analyzed with home-made programs based on MATLAB®. The EPR spectra were analyzed using the EasySpin toolbox.[80]

Magnetic measurements

Magnetic susceptibility measurements were performed using a Quantum Design MPMS2 SQUID magnetometer. Measurements were performed on powder samples of CuDPA (46.7 mg) using a gelatin capsule as sample holder with a small (and known) diamagnetic contribution at 50 mT in the temperature range of 1.8 and 250 K. The contribution of the gelatin capsule was subtracted from the measured values. The molar magnetic susceptibility values were corrected for diamagnetism using the Pascal's constants.[81]

Author contributions

A. L. P., Investigation, formal analysis, writing – original draft. Prepared the samples and performed general characterizations of the compounds, analysed EPR data, wrote the MS. A. K. and M. M. C., Data curation, investigation: prepared the samples and performed general characterizations of the compounds. S. S. and R. B., Investigation, formal analysis, resources, writing – original draft: acquired and analysed X-ray data, wrote the MS. A. F. C. and J. M. L. M., Investigation, formal analysis, resources, writing – original draft: acquired and analysed ATR-FTIR data, performed computational calculations, and wrote the MS. C. A. R. and M. V. M., Investigation, resources: performed magnetic measurements and analysed the data. C. D. B., Conceptualization, formal analysis,

resources, funding acquisition, supervision, writing – review & editing. Analysed EPR data.

Conflicts of interest

There are no conflicts to declare.

Data availability

The data supporting this article have been included as part of the ESI.†

Acknowledgements

We thank FONCyT, CONICET, and CAI+D-UNL for financial support. A. L . P., J. M. L. M., M. V. M., and C. D. B. are members of CONICET-Argentina. The author(s) are grateful to the FAIRE programme provided by the Cambridge Crystallographic Data Centre (CCDC) for the opportunity to use the Cambridge Structural Database (CSD) and associated software.

References

1 M. A. Domański and W. Grochala, *Z. Naturforsch., B: J. Chem. Sci.*, 2021, **76**, 751–758.
2 M. Fourmigué, *Acc. Chem. Res.*, 2004, **37**, 179–186.
3 L. K. Thompson and S. S. Tandon, *Comments Inorg. Chem.*, 1996, **18**, 125–144.
4 M. G. F. Vaz and M. Andruh, *Coord. Chem. Rev.*, 2021, **427**, 213611.
5 L. A. Curtiss, C. A. Naleway and J. R. Miller, *Chem. Phys.*, 1993, **176**, 387–405.
6 S. I. Levchenkov, I. N. Shcherbakov, L. D. Popov, V. V. Lukov, V. V. Minin, Z. A. Starikova, E. V. Ivannikova, A. A. Tsaturyan and V. A. Kogan, *Inorg. Chim. Acta*, 2013, **405**, 169–175.
7 M. Atzori, A. Serpe, P. Deplano, J. A. Schlueter and M. Laura Mercuri, *Inorg. Chem. Front.*, 2015, **2**, 108–115.
8 M. H. Whangbo, H. J. Koo and R. K. Kremer, *Molecules*, 2021, **26**, 531.
9 D.-T. Chen, J. Chen, X.-G. Li, G. Christou, S. Hill, X.-G. Zhang and H.-P. Cheng, *J. Phys. Chem. C*, 2021, **125**, 11124–11131.
10 E. Ruiz, A. Rodríguez-Fortea and S. Alvarez, *Inorg. Chem.*, 2003, **42**, 4881–4884.
11 M. Jung, A. Sharma, D. Hinderberger, S. Braun, U. Schatzschneider and E. Rentschler, *Inorg. Chem.*, 2009, **48**, 7244–7250.
12 J. Larionova, M. Gross, M. Pilkington, H. Andres, H. Stoeckli-Evans, H. U. Güdel and S. Decurtins, *Angew. Chem., Int. Ed.*, 2000, **39**, 1605–1609.
13 T. Cheng, D. X. Shen, M. Meng, S. Mallick, L. Cao, N. J. Patmore, H. L. Zhang, S. F. Zou, H. W. Chen, Y. Qin, Y. Y. Wu and C. Y. Liu, *Nat. Commun.*, 2019, **10**, 1531.
14 K. T. Mahmudov, M. N. Kopylovich, M. F. C. Guedes da Silva and A. J. L. Pombeiro, *Coord. Chem. Rev.*, 2017, **345**, 54–72.
15 V. F. Oswald, J. L. Lee, S. Biswas, A. C. Weitz, K. Mittra, R. Fan, J. Li, J. Zhao, M. Y. Hu, E. E. Alp, E. L. Bominaar, Y. Guo, M. T. Green, M. P. Hendrich and A. S. Borovik, *J. Am. Chem. Soc.*, 2020, **142**, 11804–11817.
16 S. J. Grabowski, *J. Phys. Chem. A*, 2007, **111**, 13537–13543.
17 J. C. Monroe, M. A. Carvajal, M. Deumal, C. P. Landee, M. Rademeyer and M. M. Turnbull, *Inorg. Chem.*, 2020, **59**, 6319–6331.
18 O. Farver and I. Pecht, *FASEB J.*, 1991, **5**, 2554–2559.
19 J.-M. Moulis, *Biomolecules*, 2020, **10**, 1584.
20 P. J. González, M. G. Rivas, F. M. Ferroni, A. C. Rizzi and C. D. Brondino, *Coord. Chem. Rev.*, 2021, **449**, 214202.
21 B. Wang, P. Wu and S. Shaik, *J. Phys. Chem. Lett.*, 2022, **13**, 2871–2877.
22 A. Varadwaj, P. R. Varadwaj, H. M. Marques and K. Yamashita, *Int. J. Mol. Sci.*, 2022, **23**, 8816.
23 Y. Chi, Q. Yuan, Y. Li, L. Zhao, N. Li, X. Li and W. Yan, *J. Hazard. Mater.*, 2013, **262**, 404–411.
24 L. M. Rossi, N. J. S. Costa, F. P. Silva and R. Wojcieszak, *Green Chem.*, 2014, **16**, 2906–2933.
25 D. K. Smith, *Chem. Rec.*, 2021, **21**, 2488–2501.
26 J. Gracia, R. Sharpe and J. Munarriz, *J. Catal.*, 2018, **361**, 331–338.
27 W. Zhou, M. Chen, M. Guo, A. Hong, T. Yu, X. Luo, C. Yuan, W. Lei and S. Wang, *Nano Lett.*, 2020, **20**, 2923–2930.
28 M. Liu, Y. Ye, J. Ye, T. Gao, D. Wang, G. Chen and Z. Song, *Magnetochemistry*, 2023, **9**, 110.
29 Y. Su, Z. Wang, R. Gao, Q. Wu, J. Zhao, G. Zhu, Q. Li, H. Xu, Y. Pan, K. Gu, C. Biz, M. Fianchini and J. Gracia, *Adv. Funct. Mater.*, 2024, **34**, 2311618.
30 C. Desplanches, E. Ruiz, A. Rodríguez-Fortea and S. Alvarez, *J. Am. Chem. Soc.*, 2002, **124**, 5197–5205.
31 G. V. R. Chandramouli, T. K. Kundu and P. T. Manoharan, *Aust. J. Chem.*, 2003, **56**, 1239–1248.
32 M. V. Fedin, S. L. Veber, K. Y. Maryunina, G. V. Romanenko, E. A. Suturina, N. P. Gritsan, R. Z. Sagdeev, V. I. Ovcharenko and E. G. Bagryanskaya, *J. Am. Chem. Soc.*, 2010, **132**, 13886–13891.
33 W. Plass, A. Pohlmann and J. Rautengarten, *Angew. Chem., Int. Ed.*, 2001, **40**, 4207–4210.
34 N. A. G. Bandeira and B. L. Guennic, *J. Phys. Chem. A*, 2012, **116**, 3465–3473.
35 B. Kozlevčar, N. Kitanovski, Z. Jagličić, N. A. G. Bandeira, V. Robert, B. Le Guennic and P. Gamez, *Inorg. Chem.*, 2012, **51**, 3094–3102.
36 I. Nemec, R. Herchel, T. Šilha and Z. Trávníček, *Dalton Trans.*, 2014, **43**, 15602–15616.
37 M. Peric, M. Zlatar, S. Grubisic and M. Gruden-Pavlovic, *Polyhedron*, 2012, **42**, 89–94.

38 F. A. Tezcan, B. R. Crane, J. R. Winkler and H. B. Gray, *Proc. Natl. Acad. Sci. U. S. A.*, 2001, **98**, 5002–5006.
39 J. A. Fereiro, X. Yu, I. Pecht, M. Sheves, J. C. Cuevas and D. Cahen, *Proc. Natl. Acad. Sci. U. S. A.*, 2018, **115**, E4577–E4583.
40 X. Zheng, D. M. Medvedev and A. A. Stuchebrukhov, *Int. J. Quantum Chem.*, 2005, **102**, 473–479.
41 A. D. L. Lande, N. S. Babcock, J. Řezáč, B. Lévy, B. C. Sanders and D. R. Salahub, *Phys. Chem. Chem. Phys.*, 2012, **14**, 5902–5918.
42 D. V. Matyushov, *J. Chem. Phys.*, 2013, **139**, 025102.
43 A. Migliore, S. Corni, R. Di Felice and E. Molinari, *J. Phys. Chem. B*, 2007, **111**, 3774–3781.
44 J. Lin, I. A. Balabin and D. N. Beratan, *Science*, 2005, **310**, 1311–1313.
45 O. Miyashita, M. Y. Okamura and J. N. Onuchic, *Proc. Natl. Acad. Sci. U. S. A.*, 2005, **102**, 3558–3563.
46 J. Li, Y. Shi and T. Cheng, *Phys. Chem. Chem. Phys.*, 2023, **25**, 16201–16211.
47 H. Mori, S. Yokomori, S. Dekura and A. Ueda, *Chem. Commun.*, 2022, **58**, 5668–5682.
48 B. D. Ratner and R. A. Latour, in *Biomaterials Science*, ed. W. R. Wagner, S. E. Sakiyama-Elbert, G. Zhang and M. J. Yaszemski, Academic Press, 4th edn, 2020, pp. 77–82.
49 V. N. Serezhkin, A. V. Vologzhanina, L. B. Serezhkina, E. S. Smirnova, E. V. Grachova, P. V. Ostrova and M. Y. Antipin, *Acta Crystallogr., Sect. B:Struct. Sci.*, 2009, **65**, 45–53.
50 E. E. Sileo, M. A. Blesa, G. Rigotti, B. E. Rivero and E. E. Castellano, *Polyhedron*, 1996, **15**, 4531–4540.
51 H.-Y. Wu, N. Wang, S.-T. Yue and Y.-L. Liu, *J. Coord. Chem.*, 2009, **62**, 2511–2519.
52 E. E. Sileo, D. Vega, M. T. Garland, R. Baggio and M. A. Blesa, *Aust. J. Chem.*, 1999, **52**, 205–212.
53 N. Okabe and N. Oya, *Acta Crystallogr., Sect. C: Cryst. Struct. Commun.*, 2000, **56**(Pt 3), 305–307.
54 M. Mirzaei, H. Eshtiagh-Hosseini, Z. Karrabi, K. Molčanov, E. Eydizadeh, J. T. Mague, A. Bauzá and A. Frontera, *CrystEngComm*, 2014, **16**, 5352–5363.
55 A. L. Pérez, A. Kemmerer, R. Baggio, C. A. Ramos, S. D. Dalosto, M. C. G. Passeggi, A. C. Rizzi and C. D. Brondino, *Eur. J. Inorg. Chem.*, 2021, **2021**, 4183–4195.
56 A. L. Pérez, N. I. Neuman, R. Baggio, C. A. Ramos, S. D. Dalosto, A. C. Rizzi and C. D. Brondino, *Polyhedron*, 2017, **123**, 404–410.
57 S. Cui, Y. Zhao, J. Zhang, Q. Liu and Y. Zhang, *Cryst. Growth Des.*, 2008, **8**, 3803–3809.
58 C.-C. Su and S.-Y. Chiu, *Polyhedron*, 1996, **15**, 2623–2631.
59 C. Xie, Z. Zhang, X. Wang, X. Liu, G. Shen, R. Wang and D. Shen, *J. Coord. Chem.*, 2004, **57**, 1173–1178.
60 R. Kubo and K. Tomita, *J. Phys. Soc. Jpn.*, 1954, **9**, 888–919.
61 H. Aghabozorg, F. Ramezanipour, J. Soleimannejad, M. A. Sharif, A. Shokrollahi, M. Shamsipur, A. Moghimi, J. Attar Gharamaleki, V. Lippolis and A. Blake, *Pol. J. Chem.*, 2008, **82**, 487–507.
62 P. Das, S. Islam and S. K. Seth, *J. Mol. Struct.*, 2024, **1308**, 138088.
63 T. Akitsu, S. Suda and N. Katsuumi, *Edelweiss Chem. Sci. J.*, 2021, 27–29, DOI: **10.33805/2641-7383.129**.
64 C. Groom, I. Bruno, M. Lightfoot and S. Ward, *Acta Crystallogr., Sect. B: Struct. Sci., Cryst. Eng. Mater.*, 2016, **72**, 171–179.
65 M. Kalinowska, M. Borawska, R. Świsłocka, J. Piekut and W. Lewandowski, *J. Mol. Struct.*, 2007, **834–836**, 419–425.
66 K. McCann and J. Laane, *J. Mol. Struct.*, 2008, **890**, 346–358.
67 G. Świderski, H. Lewandowska, R. Świsłocka, S. Wojtulewski, L. Siergiejczyk, A. Z. Wilczewska and I. Misztalewska, *Arabian J. Chem.*, 2019, **12**, 4414–4426.
68 S. K. Hoffmann, W. Hilczer and J. Goslar, *Appl. Magn. Reson.*, 1994, **7**, 289–321.
69 P. W. Anderson and P. R. Weiss, *Rev. Mod. Phys.*, 1953, **25**, 269–276.
70 C. D. Brondino, N. M. C. Casado, M. C. G. Passeggi and R. Calvo, *Inorg. Chem.*, 1993, **32**, 2078–2084.
71 P. R. Levstein, C. A. Steren, A. M. Gennaro and R. Calvo, *Chem. Phys.*, 1988, **120**, 449–459.
72 Y.-H. Chi, J.-M. Shi, H.-N. Li, W. Wei, E. Cottrill, N. Pan, H. Chen, Y. Liang, L. Yu, Y.-Q. Zhang and C. Hou, *Dalton Trans.*, 2013, **42**, 15559–15569.
73 M. M. González, H. Osiry, M. Martínez, J. Rodríguez-Hernández, A. A. Lemus-Santana and E. Reguera, *J. Magn. Magn. Mater.*, 2019, **471**, 70–76.
74 R. A. Marcus and N. Sutin, *Biochim. Biophys. Acta, Rev. Bioenerg.*, 1985, **811**, 265–322.
75 Agilent, *CrysAlis PRO*, Agilent Technologies Ltd, Yarnton, Oxfordshire, England, 2014.
76 D. J. Fox, M. J. Frisch, G. W. Trucks, H. B. Schlegel, G. E. Scuseria, M. A. Robb, J. R. Cheeseman, G. Scalmani, V. Barone, G. A. Petersson, H. Nakatsuji, X. Li, M. Caricato, A. V. Marenich, J. Bloino, B. G. Janesko, R. Gomperts, B. Mennucci, H. P. Hratchian and J. V. Ortiz, *Gaussian 16*, 2016.
77 C. Lee, W. Yang and R. G. Parr, *Phys. Rev. B: Condens. Matter Mater. Phys.*, 1988, **37**, 785–789.
78 A. D. Becke, *J. Chem. Phys.*, 1993, **98**, 5648–5652.
79 J. M. Schveigkardt, A. C. Rizzi, O. E. Piro, E. E. Castellano, R. Costa de Santana, R. Calvo and C. D. Brondino, *Eur. J. Inorg. Chem.*, 2002, 2913–2919.
80 S. Stoll and A. Schweiger, *J. Magn. Reson.*, 2006, **178**, 42–55.
81 O. Kahn, *Molecular Magnetism*, VCH Publishers, New York, 1993.